Journal of Physics and Chemistry of Solids 153 (2021) 109994

Contents lists available at ScienceDirect

Journal of Physics and Chemistry of Solids

journal homepage: http://www.elsevier.com/locate/jpcs

Iron oxidation state in $La_{0.7}Sr_{1.3}Fe_{0.7}Ti_{0.3}O_4$ and $La_{0.5}Sr_{1.5}Fe_{0.5}Ti_{0.5}O_4$ layered perovskites: Magnetic properties

T.P. Gavrilova [a,*], A.R. Yagfarova [b], Yu.A. Deeva [c], I.V. Yatsyk [a,b], I.F. Gilmutdinov [b], M. A. Cherosov [b], F.G. Vagizov [b], T.I. Chupakhina [c], R.M. Eremina [a,b]

[a] Zavoisky Physical-Technical Institute, FRC Kazan Scientific Center of RAS, 420029, Kazan, Sibirsky Tract, 10/7, Russia
[b] Institute of Physics, Kazan Federal University, 420008, Kazan, Kremlyovskaya Street18, Russia
[c] Institute of Solid State Chemistry of the Russian Academy of Sciences (UB), Pervomaiskaya St., 91, Ekaterinburg, 620990, Russia

ARTICLE INFO

Keywords:
Layered perovskite
Electronic phase separation
Fe4+
Magnetization
Electron spin resonance
Mossbauer spectroscopy

ABSTRACT

$La_{0.5}Sr_{1.5}Fe_{0.5}Ti_{0.5}O_4$ and $La_{0.7}Sr_{1.3}Fe_{0.7}Ti_{0.3}O_4$ solid solutions with the layered perovskite structure were synthesized using a solid state method. Structural properties of obtained samples were characterized using X-ray diffraction and X-ray fluorescence analyses. Magnetic properties were investigated using magnetometry, electron spin resonance (ESR) and Mössbauer spectroscopy methods. Based on magnetization and ESR measurements it was suggested the presence of Fe^{4+} ions in addition to trivalent iron ions that was exactly confirmed by Mössbauer spectroscopy investigations. Based on all experimental results one can suggest the presence of the electronic phase separation in the investigated samples – the simultaneous existence of the paramagnetic phase and magnetically correlated regions, which form due to the mixed-valence iron ions. So the paramagnetic phase with strong antiferromagnetic correlation exists in both samples, while the second phase is ferromagnetically and ferrimagnetically correlated regions in $La_{0.5}Sr_{1.5}Fe_{0.5}Ti_{0.5}O_4$ and $La_{0.7}Sr_{1.3}Fe_{0.7}Ti_{0.3}O_4$, respectively.

1. Introduction

Layered perovskite structures with the chemical formula A_2BO_4, (where A is a rare earth or alkaline earth element, and B is - d-metals of the IV period of the periodic table), are widely known and intensively studied, since they possess a multifunctional set of properties that are promising for practical applications. Recently interest in these compounds was increased due to new synthesis methods and experimental results demonstrating the possible using in energy-storage devices, including negative electrodes for advanced Li-ion batteries [1], for low-loss microwave dielectric applications and many others [2]. So the giant dielectric permittivity was found in strontium nickelates which were considered until 2009 as low-resistance semiconductors [3,4]. It is known that $La_{0.6}Sr_{1.4}MnO_4$ has the largest magnetoresistance ratio ($[\rho(H)-\rho(0)]/\rho(0)$), which reaches to 78.4% at 48 K [5], while $La_{2-x}Sr_xCuO_4$ is a superconducting material [6], Sr_2CoO_4 is a ferromagnetic metal with the ferromagnetic–paramagnetic transition Curie temperature $T_C \approx 250$ K [7]. Strontium titanate Sr_2TiO_4 is considered as a dielectric material with a high Q factor [8] and a photocatalyst [9] or a luminophore in the case of doping in the A position with rare earth elements such as Eu, Gd and others [10].

In the A_2BO_4 structure, the ABO_3 layers with the perovskite structure are separated by A - O layers of rock salt, and the B–O – B electronic interactions can occur only in the plane. Variations in electrical, magnetic, catalytic, and other properties are possible both by isomorphic substitution of cations in the B positions, and by conjugate substitution in the B and A positions. So Sr_2TiO_4 is a diamagnetic dielectric material (A_2BO_4 structure with B═ Ti^{4+}, $3d^0$), while the inclusion of La/Fe in the oxide composition significantly improves the optical absorption of Sr_2TiO_4 in the visible region of the spectrum due to the formation of additional spin-polarized bands (SPBs) within the initial band gap of Sr_2TiO_4, so the complex oxide $Sr_{1.7}La_{0.3}Ti_{0.7}Fe_{0.3}O_4$ is recommended for use in the photocatalytic decomposition of water [11]. From the point of view of dielectric properties $Sr_{2-x}La_xTi_{1-x}Fe_xO_4$ (x = 0.5 и 0.7) are materials with a high dielectric constant $\varepsilon \approx 10^5$ [12]. One of the reasons for the high values of the dielectric constant of these oxides is small polaron hopping conduction mechanism presumably due to the different valence state of Fe. One can suggest that observed in strontium titanate (with conjugated La/Fe substitution in positions A and B) effects can be due to the presence of half-filled d-orbitals of Fe^{3+} ions, which are usually in a

* Corresponding author.
E-mail address: tatyana.gavrilova@gmail.com (T.P. Gavrilova).

https://doi.org/10.1016/j.jpcs.2021.109994
Received 22 October 2020; Received in revised form 25 January 2021; Accepted 5 February 2021
Available online 9 February 2021

high spin state, as well as the probability of the existence of mixed-valence iron ions. Thus a deep understanding and explanation of properties such as photocatalytic activity and high dielectric constant in $Sr_{2-x}La_xTi_{1-x}Fe_xO_4$ (x = 0.5 и 0.7) oxides requires a detailed investigation of their magnetic properties. Here we present the magnetometry, electron spin resonance and Mössbauer spectroscopy measurements of $La_xSr_{2-x}Fe_xTi_{1-x}O_4$ (x = 0.5 и 0.7) oxides to prove the existence of mixed-valence iron ions and study the associated effects.

2. Synthesis and experimental details

The synthesis of $La_xSr_{2-x}Fe_xTi_{1-x}O_4$ (x = 0.5 and 0.7) complex oxides was carried out by the nitrate - citrate method with the addition of diammonium citrate as an organic component owing to procedure described in Ref. [13]. The final firing temperature of the compact pressed sample was 1300 °C.

Phase formation process was controlled by X-ray analysis using a Shimadzu XRD-7000S automatic diffractometer. X-ray pattern processing was performed according to the Rietveld method using the FULLPROF-2018 software. The X-ray fluorescence analysis (XFA) of $La_{0.5}Sr_{1.5}Fe_{0.5}Ti_{0.5}O_4$ and $La_{0.7}Sr_{1.3}Fe_{0.7}Ti_{0.3}O_4$ samples was carried out on a Bruker S2 Ranger X-ray fluorescence spectrometer.

The magnetization was measured using a commercial PPMS-9 platform (Quantum Design) in the temperature range from 5 to 300 K in zero-field-cooled (ZFC) and field-cooled (FC) regimes. The magnetic hysteresis loops were measured in the magnetic field range 2 T and in the temperature range from 2 K to 100 K. To investigate the magnetic hysteresis loops in M − H curves the magnet was demagnetized to zero field in the oscillation mode. Magnetic resonance spectra of solid solutions were measured on an ER 200 SRC (EMX/plus) spectrometer (Bruker) at the frequency of 9.4 GHz with a flow N_2 Temperature Controller RS 232 cryostat (Bruker) in the temperature range from 100 to 340 K and Temperature Controller ITC 503S (Oxford instruments) in the temperature range from 5 to 150 K.

Mössbauer measurements were performed using a conventional constant-acceleration setup with WisseL (Germany) electronics modules. Spectra have been recorded in transmission geometry in the temperature range 5–300 K. A ^{57}Co (Rh) commercial source (Ritverc isotope products, Saint Petersburg, Russia) was used as the γ-radiation source. Low-temperature measurements were carried out with a continuous flow cryostat (model CFICEV from ICE Oxford, UK), equipped with Cryo-Con temperature controller (Model 32B). The recorded spectra were fitted with hyperfine parameter distributions by the SpectrRelax software [14]. A metallic iron foil at RT was used for velocity calibration of the Mössbauer spectrometer. Isomer shifts were referred to α-Fe at RT.

3. Sample characterization

3.1. X-ray diffraction analysis

Experimental, theoretical, and difference X-ray diffraction patterns of $La_{0.7}Sr_{1.3}Fe_{0.7}Ti_{0.3}O_4$ sample are shown in Fig. 1. The diffraction pattern of $La_{0.5}Sr_{1.5}Fe_{0.5}Ti_{0.5}O_4$ sample has a similar profile. The performed XRD measurements showed that both samples are single-phase one and their crystal structures are indexed on the basis of space group I4/mmm (No 139). The parameters of unit cells are shown in Table 1.

3.2. X-ray fluorescence analysis

$La_{0.7}Sr_{1.3}Fe_{0.7}Ti_{0.3}O_4$ and $La_{0.5}Sr_{1.5}Fe_{0.5}Ti_{0.5}O_4$ solid solutions were investigated by X-ray fluorescence analysis (XFA) at the maximum possible resolution of the instrument at room temperature. The element selective images obtained using XFA for both samples demonstrated the uniform distribution of elements (element distribution maps and initial atomic ratio are given in supplemental materials (Table S1 and Fig. S1)).

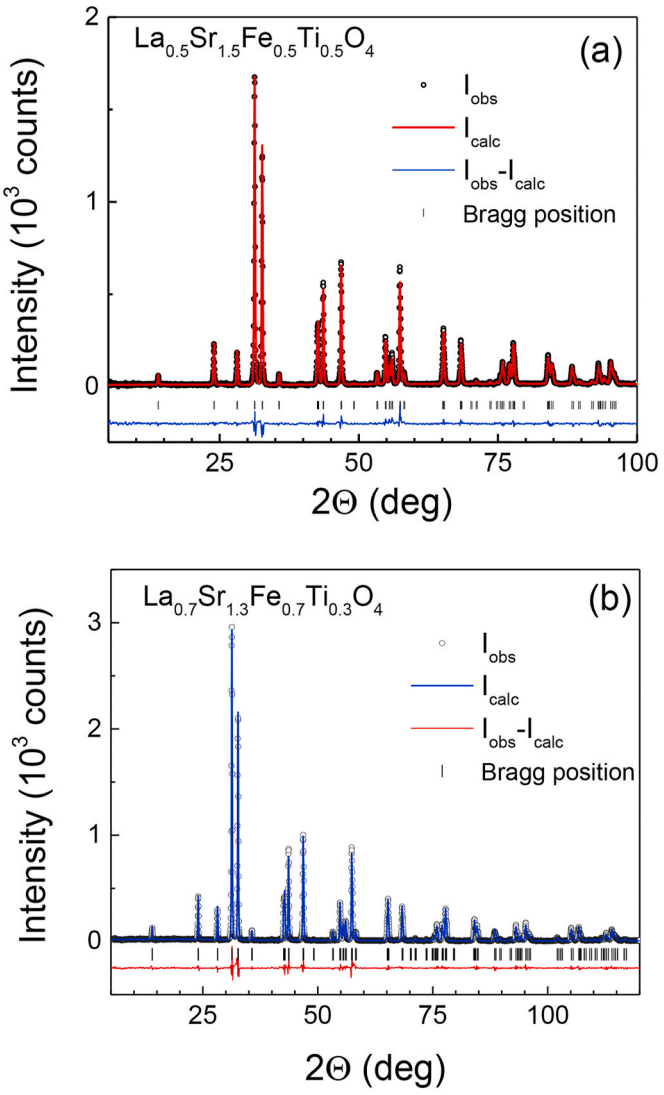

Fig. 1. Experimental, theoretical, and differential diffraction patterns of (a) $La_{0.5}Sr_{1.5}Fe_{0.5}Ti_{0.5}$ and (b) $La_{0.7}Sr_{1.3}Fe_{0.7}Ti_{0.3}O_4$.

Table 1
Unit cell parametres of $La_xSr_{2-x}Fe_xTi_{1-x}O_4$ (x = 0.5 and 0.7) oxides, space group I4/mmm.

Unit cell parameters	x = 0.5	x = 0.7
$a = b$, Å	3.8802 (1)	3.8807 (1)
c, Å	12.6705 (1)	12.6905 (3)
V, Å^3	190.765 (7)	191.117 (8)

Table 2 summarizes the average concentration ratio between elements for investigated samples. From Table 2 it can be seen that the average composition of the samples is close to the composition expected from the initial synthesis process.

In the end of discussion we should note that both samples have a granular structure with an average grain size of 1.2 μm and 1.38 μm for $La_{0.5}Sr_{1.5}Fe_{0.5}Ti_{0.5}O_4$ and $La_{0.7}Sr_{1.3}Fe_{0.7}Ti_{0.3}O_4$, respectively (Fig. 1 in Ref. [12]). We suggest that the size of the granules is large enough to exclude the influence of size effects on the magnetic properties of the samples.

Table 2
The average element composition of $La_{0.7}Sr_{1.3}Fe_{0.7}Ti_{0.3}O_4$ and $La_{0.5}Sr_{1.5}Fe_{0.5}Ti_{0.5}O_4$ samples (XFA data).

data source\ element	$\frac{La}{La+Sr+Fe+Ti}$	$\frac{Sr}{La+Sr+Fe+Ti}$	$\frac{Fe}{La+Sr+Fe+Ti}$	$\frac{Ti}{La+Sr+Fe+Ti}$
		$La_{0.7}Sr_{1.3}Fe_{0.7}Ti_{0.3}O_4$		
initial values	0.23	0.43	0.23	0.1
XFA	0.19	0.53	0.2	0.08
		$La_{0.5}Sr_{1.5}Fe_{0.5}Ti_{0.5}O_4$		
initial values	0.17	0.5	0.17	0.17
XFA	0.16	0.56	0.17	0.11

4. Experimental results

4.1. Magnetization

The magnetization of $La_{0.7}Sr_{1.3}Fe_{0.7}Ti_{0.3}O_4$ and $La_{0.5}Sr_{1.5}Fe_{0.5}Ti_{0.5}O_4$ solid solutions as a function of temperature (M-T curve) was measured in magnetic fields of H = 0.1 T in FC regime (Fig. 2) and in magnetic field H = 10 mT in FC and ZFC regimes (Fig. 3). The magnetization of $La_{0.5}Sr_{1.5}Fe_{0.5}Ti_{0.5}O_4$and $La_{0.7}Sr_{1.3}Fe_{0.7}Ti_{0.3}O_4$ samples as a function of magnetic field (M − H curve) was measured at different temperatures and it is presented in details in Fig. S2 and Fig. 4.

From Fig. 4 and Fig. S2 one can see that the magnetization is not saturated in the investigated magnetic field range even at T = 2 K. This fact suggests most of the sample is in paramagnetic state. At the same time the ferromagnetic nature of the hysteresis loops suggests the presence of magnetically correlated regions simultaneously with the paramagnetic phase. Since the magnetization is the total characteristic of the entire sample and it is not possible to separate experimentally the paramagnetic and ferromagnetic contributions to the magnetization data (M − H curve at low temperatures) can be considered as a sum of the ferromagnetic and paramagnetic contributions:

$$M(H) = M_{FM}(H) + M_{PM}(H) \quad (1)$$

where the paramagnetic contribution is $M_{PM}(H) = \chi \cdot H$, while the ferromagnetic hysteresis loop is given by Refs. [15,16]:

$$M_{FM}(H) = \frac{2M_S}{\pi} tan^{-1}\left(\frac{H \pm H_C}{H_T}\right) \quad (2)$$

where M_S is the saturation magnetization, H_C is the coercive field, H is the external magnetic field and H_T is the threshold field that has to be exceeded to saturate the sample magnetically. The obtained fitting parameters are listed in Table 3. The calculated using Eqs. (1) and (2) theoretical curves are presented in Fig. 4 by solid lines.

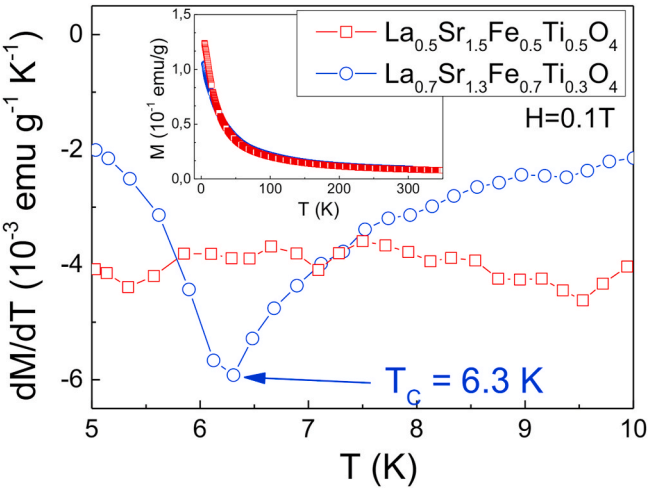

Fig. 2. Temperature dependencies of the first derivative of the magnetization for $La_{0.7}Sr_{1.3}Fe_{0.7}Ti_{0.3}O_4$ and $La_{0.5}Sr_{1.5}Fe_{0.5}Ti_{0.5}O_4$ measured in FC regime in the external magnetic field H = 0.1 T. Inset shows the temperature dependence of the magnetization of both samples [12].

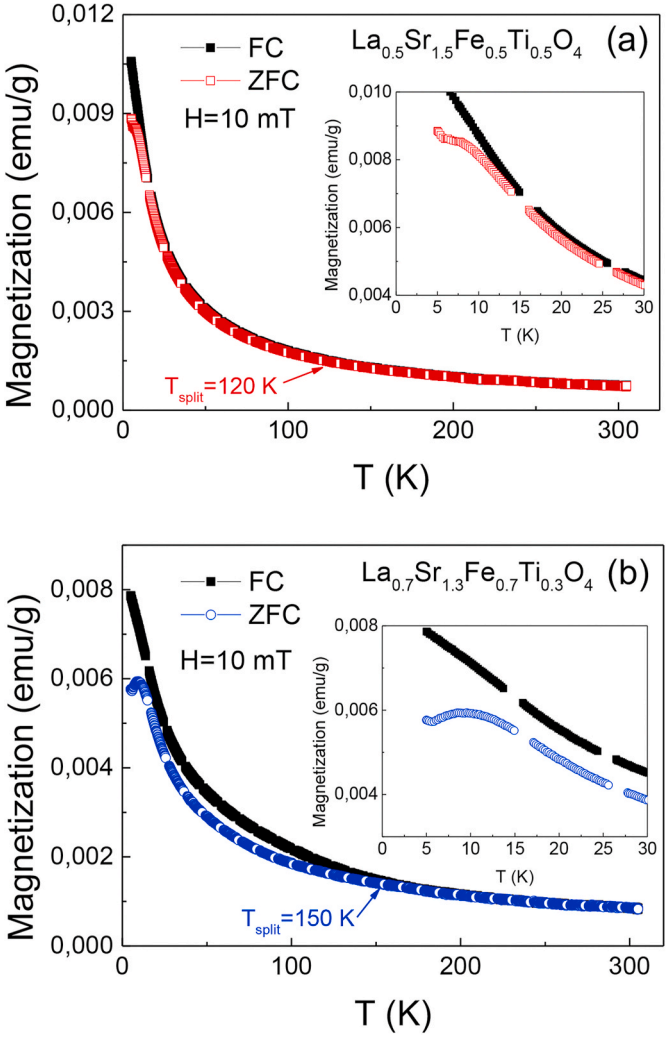

Fig. 3. Temperature dependence of magnetization in: (a) $La_{0.5}Sr_{1.5}Fe_{0.5}Ti_{0.5}O_4$ and (b) $La_{0.7}Sr_{1.3}Fe_{0.7}Ti_{0.3}O_4$ measured in FC, ZFC regimes in the external magnetic field H = 10 mT. Insets show the low temperature data in more detail.

4.2. Electron spin resonance

The typical electron spin resonance spectra of the investigated samples $La_{0.5}Sr_{1.5}Fe_{0.5}Ti_{0.5}O_4$ and $La_{0.7}Sr_{1.3}Fe_{0.7}Ti_{0.3}O_4$ at different temperatures are presented in Fig. 5. The broad line observed in ESR spectra is related to Fe^{3+} ions ($3d^5$, S = 5/2). The absence of the fine structure of Fe^{3+} ion in the ESR spectra of $La_{0.5}Sr_{1.5}Fe_{0.5}Ti_{0.5}O_4$ and $La_{0.7}Sr_{1.3}Fe_{0.7}Ti_{0.3}O_4$ can be associated with the presence of exchange interactions between spins of iron ions. Exchange interactions between

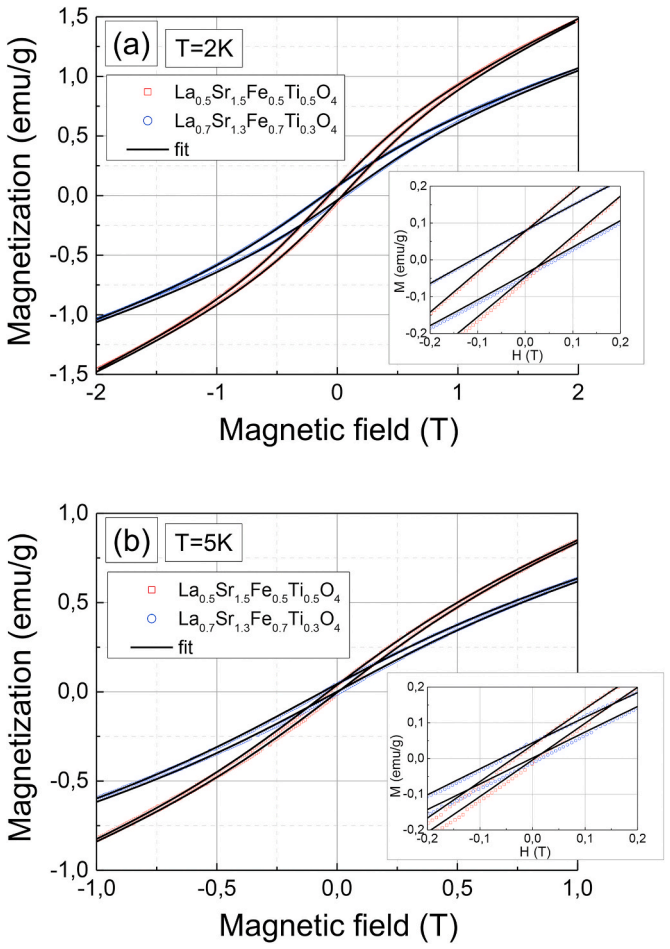

Fig. 4. Magnetization as a function of the external magnetic field in $La_{0.5}Sr_{1.5}Fe_{0.5}Ti_{0.5}O_4$ and $La_{0.7}Sr_{1.3}Fe_{0.7}Ti_{0.3}O_4$ solid solutions at: (a) T = 2 K and (b) T = 5 K. Solid lines corresponds to the fitting using Eqs. (1) and (2). Insets show the same data on a larger scale.

Table 3
Hysteresis loop characteristics of $La_{0.5}Sr_{1.5}Fe_{0.5}Ti_{0.5}O_4$ and $La_{0.7}Sr_{1.3}Fe_{0.7}Ti_{0.3}O_4$ solid solutions.
M_S is given in 10^{-3} emu/g and χ is given in 10^{-3} emu/(g•Oe), H_C and H_T are given in mT.

T (K)	H_C (left)	H_C (rigth)	H_T	M_S	χ
		$La_{0.5}Sr_{1.5}Fe_{0.5}Ti_{0.5}O_4$			
2	115	68	771	823	422
5	65	7	702	644	445
		$La_{0.7}Sr_{1.3}Fe_{0.7}Ti_{0.3}O_4$			
2	192	90	946	619	306
5	82	−9	1072	800	237

magnetic ions in such magnetically concentrated compounds lead to the merging of the fine-structure lines into a single absorption [17]. The Fe^{4+} ($3d^4$, S = 2) iron ion, which is presented in $La_{0.5}Sr_{1.5}Fe_{0.5}Ti_{0.5}O_4$ and $La_{0.7}Sr_{1.3}Fe_{0.7}Ti_{0.3}O_4$ samples according to Mössbauer spectroscopy data, has the singlet ground-state and is an ESR-nonactive ion. The population of higher energy levels and the direct observation of Fe^{4+} ion in ESR spectra are possible at higher temperatures than it was in our experiments. At the same time we can detect the influence of the exchange interaction between Fe^{3+} and Fe^{4+} on the ESR lineshape as an additional absorption line from the magnetically correlated regions formed due to exchange interaction between Fe^{3+} and Fe^{4+} ions (line 2).

The observed ESR absorption is well described by the sum of two field derivative of a Lorentzian line with resonance field H_{res} and half

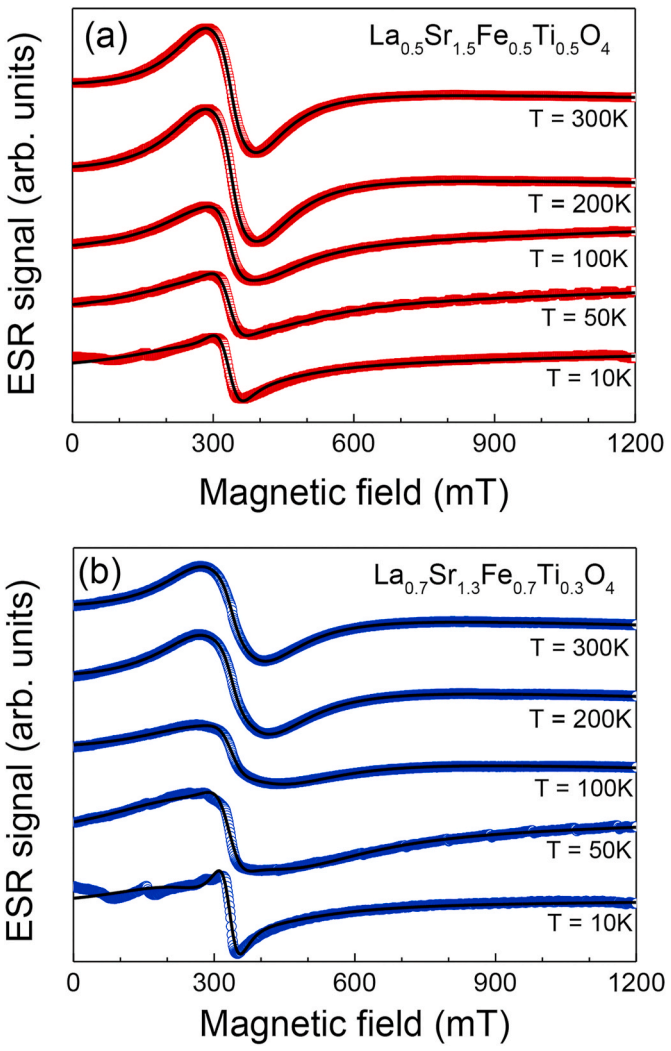

Fig. 5. Typical ESR spectra of (a) $La_{0.5}Sr_{1.5}Fe_{0.5}Ti_{0.5}O_4$ and (b) $La_{0.7}Sr_{1.3}Fe_{0.7}Ti_{0.3}O_4$ at X-band frequency (9.4 GHz) at different temperatures. Symbols indicates experimental data, solid lines indicate fits by the sum of two field derivative of a Lorentz curve.

width at half maximum linewidth ΔH within the whole temperature range. The decomposition details of magnetic resonance spectra are given in supplemental materials (Fig. S3). Temperature dependencies of parameters of ESR spectra (resonance field H_{res}, linewidth ΔH, integral intensity I) are shown in Fig. 6. The normalized integral intensity was obtained as the integral intensity $I = A \cdot \Delta H^2$ (A - signal amplitude, ΔH – ESR linewidth) divided by the maximum value for two lines I_{max} to be able to compare the integrated intensities of the two components of the ESR spectrum with each other.

We suggest that the first line (dependencies with index 1 in Fig. 6) is a signal from a paramagnetic phase in investigated samples at high temperatures: T > 120 K for $La_{0.5}Sr_{1.5}Fe_{0.5}Ti_{0.5}O_4$ and T > 150 K for $La_{0.7}Sr_{1.3}Fe_{0.7}Ti_{0.3}O_4$. This is confirmed by the typical paramagnetic behavior of ESR parameters:

(i) hyperbolic dependence of the integral intensity of ESR lines. Usually, the temperature dependence of the integral intensity coincides with the temperature behavior of the DC magnetic susceptibility $I \sim \chi$ and follows the Curie-Weiss law $I^{-1} \sim (T-\theta)$ for paramagnetic materials (Fig. 6c and d);

(ii) values of resonance fields are about $H_{res} \approx 340$ mT (it is equal to g-factor $g \approx 2$) at high temperatures (Fig. 6a), which is typical for Fe^{3+} iron ions with S = 5/2. The increasing in the resonance field and ESR linewidth with decreasing of temperature (Fig. 6a and b) can be

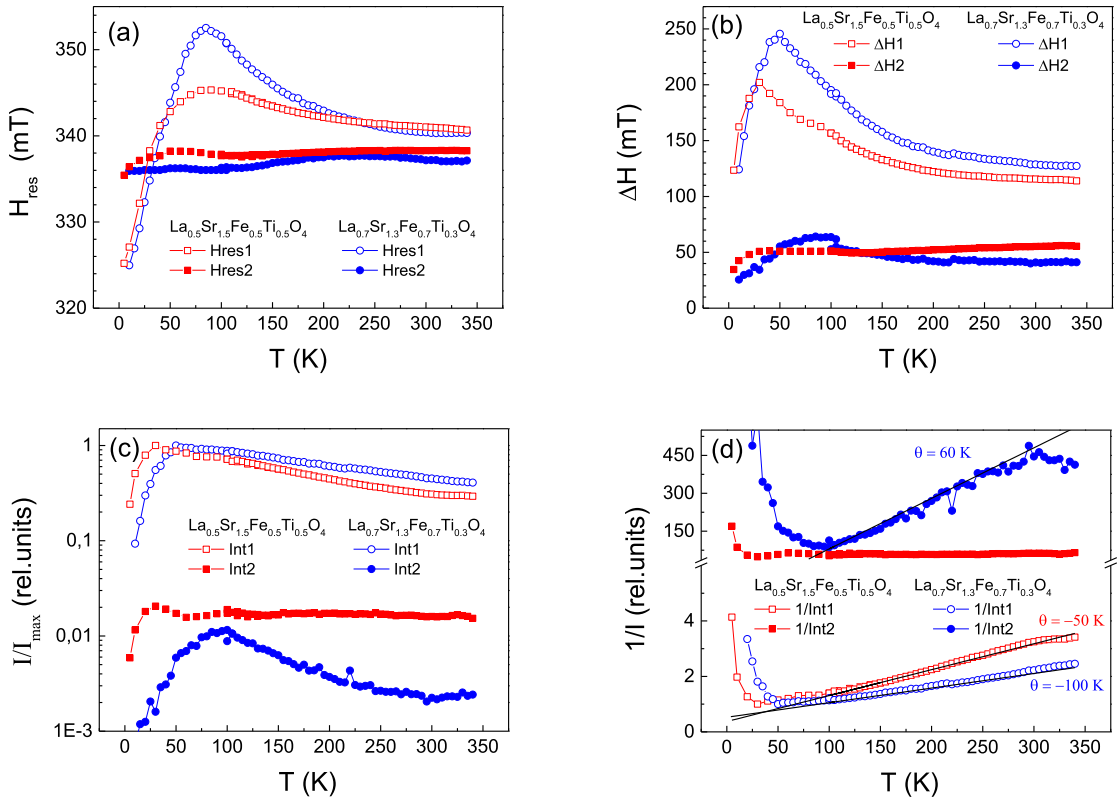

Fig. 6. Temperature dependence of (a) resonance field, (b) linewidth, (c) normalized integral intensity I/I_{max} and (d) inverse normalized integral intensity I^{-1} of two lines in ESR spectra of $La_{0.5}Sr_{1.5}Fe_{0.5}Ti_{0.5}O_4$ and $La_{0.7}Sr_{1.3}Fe_{0.7}Ti_{0.3}O_4$.

observed due to the partial transition of the system into a magnetically ordered state and the appearance of regions with a short-range magnetic order in magnetically concentrated system when approaching the magnetic phase transition temperature [18,19].

At low temperatures T < 120 K for $La_{0.5}Sr_{1.5}Fe_{0.5}Ti_{0.5}O_4$ and T < 150 K for $La_{0.7}Sr_{1.3}Fe_{0.7}Ti_{0.3}O_4$, the paramagnetic phase goes into magnetically ordered state (antiferromagnetic state), that confirms by the significant drop in the integral intensity and negative values of Weiss constants.

The temperature behavior of ESR parameters of second line (dependencies with index 2 in Fig. 6) is different for two samples. Most probably, the second line in $La_{0.5}Sr_{1.5}Fe_{0.5}Ti_{0.5}O_4$ is a signal from the ferromagnetically correlated regions containing Fe^{3+} and Fe^{4+} ions, because the position and integral intensity are independent of temperature except very low temperatures T < 25 K. For $La_{0.7}Sr_{1.3}Fe_{0.7}Ti_{0.3}O_4$, both the dependencies of the resonance field and the integral intensity of line 2 on temperature were observed. From Fig. 6c and d we can see that the integral intensity follows the Curie-Weiss law $I^{-1} \sim (T-\theta)$ with positive value of the Weiss constant θ = 60 K at high temperatures and drops down at low temperatures assuming the presence of ferrimagnetic ordering in this phase.

4.3. Mössbauer effect study

Mössbauer spectroscopy was used to determine the oxidation state of Fe ions, once this technique is very sensitive to the chemical environment around the ^{57}Fe nucleus. The room temperature Mössbauer spectra of $La_{0.5}Sr_{1.5}Fe_{0.5}Ti_{0.5}O_4$ and $La_{0.7}Sr_{1.3}Fe_{0.7}Ti_{0.3}O_4$ samples (Fig. 7) exhibit a doublet with broadened and asymmetrical lines, which indicates the presence of electric quadrupole interactions with a hyperfine parameters distributions. These spectra were fitted with hyperfine parameters distributions by the SpectrRelax software.

The reconstruction of the distribution function of the hyperfine parameters (see inserts on Fig. 7) revealed that the main part of the iron ions has an isomer shift close to 0.33 mm/s, which corresponds to trivalent iron ions Fe^{3+} in an octahedral environment. A small peak in the region of small and negative values of isomer shifts is also observed on the distribution curve, *p* (IS). These values of isomer shifts are close to the parameters given in the work [20] for iron ions in the four valence state, Fe^{4+}. It is worth pointing out that the shape of the Fe^{3+} doublet is not a simple Lorentzian, and it is likely composed of several doublets corresponding to different environments of iron ions. To verify this assumption, we performed the fitting of the experimental spectra by the SpectrRelax software to reveal the distribution of quadrupole splittings.

Fig. 8 shows the result of a best fit of the spectrum of the $La_{0.7}Sr_{1.3}Fe_{0.7}Ti_{0.3}O_4$ sample under the assumption of the hyperfine parameters distribution. As can be seen from Fig. 8, at least four components are determined in the distribution of quadrupole shifts. The existence of four or more kinds of octahedral sites for iron ions, Fe^{3+}, is in agreement with a statistical distribution of iron in the octahedral sites. This is also in agreement with the absence of any superstructure according to our X-ray data. For our samples of composition $La_{0.7}Sr_{1.3}Fe_{0.7}Ti_{0.3}O_4$ and the $La_{0.5}Sr_{1.5}Fe_{0.5}Ti_{0.5}O_4$ for each Fe^{3+} site there are five possibilities of neighbours corresponding to 4 Ti, 3 Ti + l Fe, 2 Ti + 2 Fe, 1 Ti + 3 Fe and 4 Fe, respectively. The two extreme possibilities, 4 Ti or 4 Fe, should in fact be rather low.

Hence a description of the environments of one Fe^{3+} ion by other metallic Ti ions can be proposed. It is based on a binomial distribution, in which the probability *P* (*m, x*) that one Fe^{3+} ion be surrounded by *m* Fe ions as first neighbours is given by the equation:

$$P(m,x) = \frac{4!}{m!(4-m)!}x^m(1-x)^{4-m} \quad (3)$$

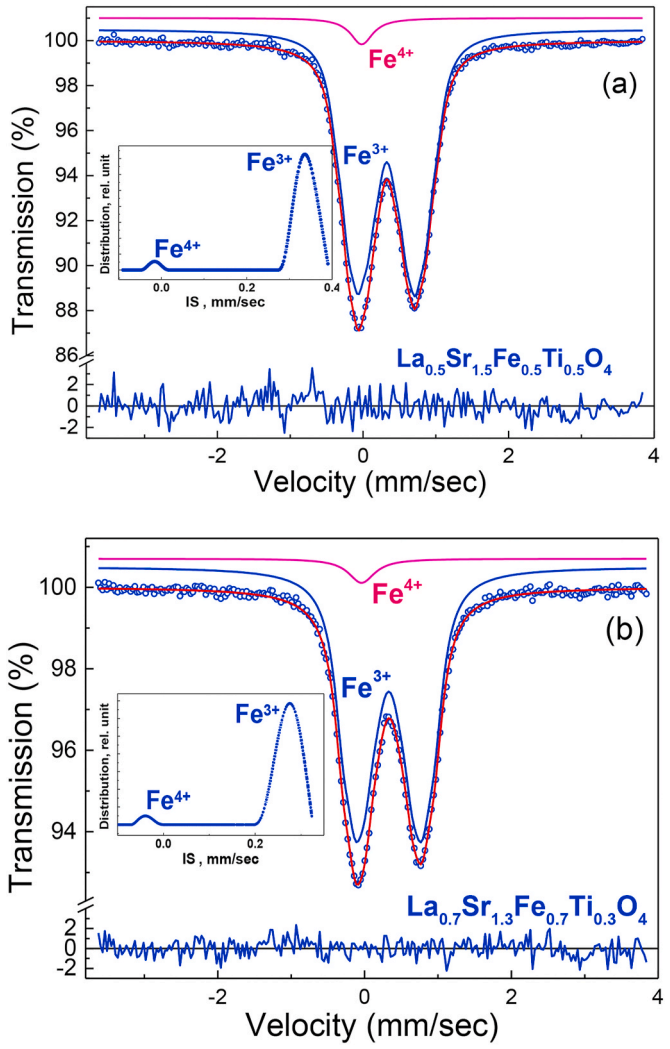

Fig. 7. Mössbauer spectra of (a) $La_{0.5}Sr_{1.5}Fe_{0.5}Ti_{0.5}O_4$ and (b) $La_{0.7}Sr_{1.3}Fe_{0.7}Ti_{0.3}O_4$ samples measured at RT and corresponding distributions of the isomer shift, p (IS).

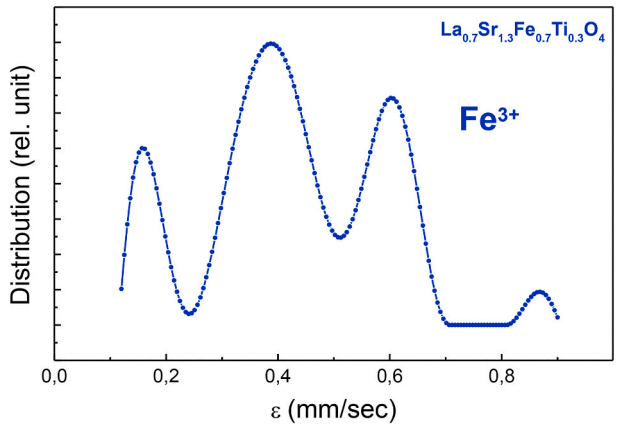

Fig. 8. The distribution of the quadrupole shifts, ε, revealed in the RT spectrum of the $La_{0.7}Sr_{1.3}Fe_{0.7}Ti_{0.3}O_4$ sample, $p(\varepsilon)$.

where (1-x) corresponds to the titanium concentration and m ranges from 0 to 4. The probabilities for the compositions $x = 0.5$ and 0.7 are shown in Table 4. The binomial distribution probability values for x = 0.7 suggest that at least the four components can be observed in the Mössbauer spectrum, which correspond to the nearest-neighbor environment of one Fe^{3+} ion having one, two, three and four other iron cations. Qualitatively, these probabilities are consistent with the distribution of quadrupole shifts shown in Fig. 8.

Table 4
Binomial distribution: the probability that an iron ion has m iron ions as first nearest-neighbours ($0 \le m \le 4$).

x	M				
	0	1	2	3	4
0.5	0.0625	0.25	0.375	0.25	0.0625
0.7	0.0081	0.0756	0.2646	0.4116	0.2401

The next step in our analysis was to verify the possibility of decomposing the experimental spectrum into separate doublets with different values of the isomer shift and quadrupole splitting. The refined values of the hyperfine parameters (IS, QS, Γ), the fitted intensities of different components and the intensities deduced from binomial distribution are given in Table 5. The revealed doublets exhibit isomer shift values in the range from 0.32 (4) to 0.33 (2) mm/s, which are characteristic for Fe^{3+}. The minor doublet with small quadrupole splitting, which have the negative isomer shift can be attributed to Fe^{4+}. As can be seen from Table 5, there is a qualitative correspondence between the experimental data and the calculated probabilities of the binomial distribution.

The doublet structure of the Mössbauer spectra of the studied samples is preserved up to low temperatures, however, starting from a temperature of the order of 100 K, a broadened magnetic sextet begins to appear in both compounds (Fig. 9).

The average center shift of doublets is found to increase as the temperature is decreased. The total change from $T = 295$ K down to $T = 80$ K is about 0.11 mm/s and 0.098 mm/s for $La_{0.7}Sr_{1.3}Fe_{0.7}Ti_{0.3}O_4$ and $La_{0.5}Sr_{1.5}Fe_{0.5}Ti_{0.5}O_4$, respectively. This variation can be mainly attributed to the relativistic temperature-dependent contribution to the isomer shift caused by the second-order Doppler shift. In the Debye approximation center shift can be expressed by Ref. [21] or [22]:

$$\delta = \delta_{IS} + \delta_{SOD} = \delta_{IS} - \frac{9k_B\theta_D}{2Mc^2}\left[\frac{1}{8} + \left(\frac{T}{\theta_D}\right)^4 \int_0^{\theta_D/T} \frac{x^3}{e^x - 1}dx\right] \quad (4)$$

where δ_{IS} - the temperature independent part of the isomer shift, i.e. it is a measure of the s-electron density at the nucleus, k_B- the Boltzmann constant, θ_D- Debye temperature, M- the mass of the ^{57}Fe atom, c- the speed of light. The solid red line in Fig. 10 represents the best fitting of the data obtained by the least-squares procedure. From the experimental results, the effective Debye temperature, θ_D is estimated to be about 543 K for $La_{0.5}Sr_{1.5}Fe_{0.5}Ti_{0.5}O_4$ solid solution, and 470 K for $La_{0.7}Sr_{1.3}Fe_{0.7}Ti_{0.3}O_4$.

5. Discussion

Our previously initial magnetization measurements of $La_{0.5}Sr_{1.5}Fe_{0.5}Ti_{0.5}O_4$ and $La_{0.7}Sr_{1.3}Fe_{0.7}Ti_{0.3}O_4$ were reported in Ref. [12] and suggested that the investigated samples are in the paramagnetic state with strong antiferromagnetic correlation between spins of magnetic ions, because above T > 200 K the M-T curve (FC regime H = 0.1 T) can be fitted by the Curie-Weiss low with negative values of the Weis constant. Moreover, in the sample with a higher iron content $La_{0.7}Sr_{1.3}Fe_{0.7}Ti_{0.3}O_4$ the sharp feature was clearly detected at the temperature about 6 K (Fig. 2), that most probably corresponds to the phase transition to the antiferromagnetically (AFM) ordered state. The phase transition to AFM state is confirmed by further ESR experiments, where the drop decrease in the integral intensity of the paramagnetic line (line 1) is

Table 5
Mössbauer parameters of the $La_xSr_{2-x}Fe_xTi_{1-x}O_4$, (x = 0.5 and 0.7) samples measured at RT.

x	IS, mm/sec	QS, mm/sec	Γ, mm/sec	% exp	valence state	*m*	% cal
0.7	0.32 (8)	0.91 (4)	0.30 (5)	34.(5)	Fe^{3+}	3	41.16
	0.33 (2)	1.23 (9)	0.30 (5)	24.(4)	Fe^{3+}	4	24.01
	0.33 (1)	0.63 (2)	0.30 (5)	26.(7)	Fe^{3+}	2	26.46
	0.32 (9)	0.31 (5)	0.30 (5)	10.(3)	Fe^{3+}	1	7.56
	−0.04 ± 0.05	-	0.27 ± 0.1	4 ± 2	Fe^{4+}		
0.5	0.32 (3)	0.78 (5)	0.25 (3)	28.(5)	Fe^{3+}	2	37.5
	0.32 (7)	1.05 (9)	0.25 (3)	24.(4)	Fe^{3+}	1	25.0
	0.32 (9)	0.52 (6)	0.25 (3)	21.(8)	Fe^{3+}	3	25.0
	0.32 (4)	0.24 (9)	0.25 (3)	11.(3)	Fe^{3+}	0	6.25
	0.32 (8)	1.36 (2)	0.25 (3)	9.(9)	Fe^{3+}	4	6.25
	−0.01 ± 0.05	-	0.37 ± 0.1	4 ± 2	Fe^{4+}		

IS - isomer shift relative to metallic iron; QS - quadrupole splitting; Γ - half-height width; % exp - fitted intensities of different components; and % cal - intensities deduced from binomial distribution.

observed below T = 50 K. In addition to above mentioned experiments the magnetization measurements in FC-ZFC regimes in low magnetic field H = 10 mT (see Ref. [12] and Fig. 3) were performed to determine the temperature below which magnetic correlations become dominant over thermal fluctuations. The ZFC-FC splitting was already observed in $La_{0.7}Sr_{1.3}Fe_{0.7}Ti_{0.3}O_4$ below T_{split} = 150 K, while in $La_{0.5}Sr_{1.5}Fe_{0.5}Ti_{0.5}O_4$ it was observed only below T_{split} = 120 K (Fig. 3). This splitting suggests the presence of short-range magnetic correlations in the investigated samples that can be proved at the next step by isothermal magnetization measurements as a function of the external magnetic field below 120–150 K (Fig. S2).

Nonlinear behavior of M − H curves was observed for both samples at T = 10 K, while the ferromagnetic hysteresis loops were clearly detected in M − H curves at temperatures 5 K and 2 K (Fig. 4, Fig. S2).

From Fig. 4 and Table 3 one can see some interesting results:

(i) hysteresis loops are not symmetric about the M axis (left and right coercive fields are different);
(ii) opposite behavior in temperature dependencies of saturation magnetization M_S and threshold field H_T for two samples (decrease of M_S and H_T for $La_{0.5}Sr_{1.5}Fe_{0.5}Ti_{0.5}O_4$ and increase for $La_{0.7}Sr_{1.3}Fe_{0.7}Ti_{0.3}O_4$ with increasing temperature).

The observed shift of the magnetic hysteresis loop is the typical manifestation of exchange bias effect [23], so one can suggest the presence of two different types of magnetic phases, which are exchange coupled to each other. Usually the shift was absent when the sample was cooled in zero field (in our case the shift was observed in ZFC regime),

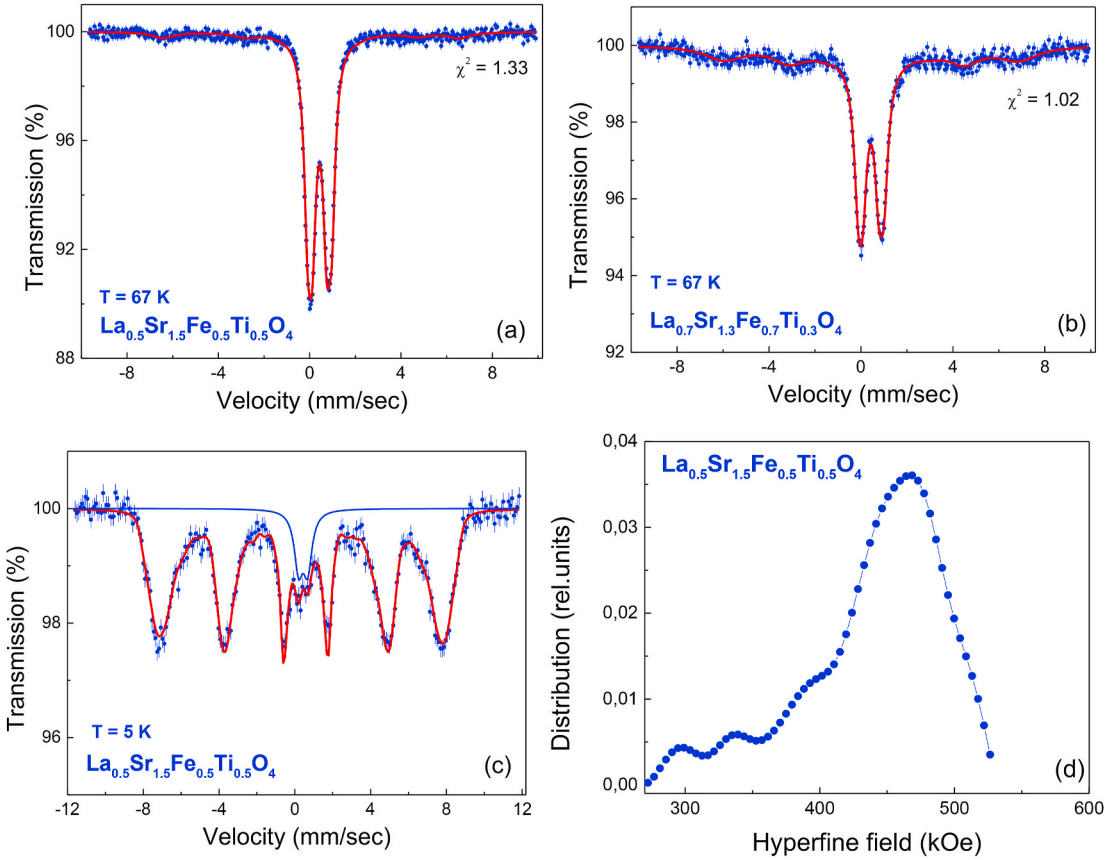

Fig. 9. Mössbauer spectra of (a) $La_{0.5}Sr_{1.5}Fe_{0.5}Ti_{0.5}O_4$ and (b) $La_{0.7}Sr_{1.3}Fe_{0.7}Ti_{0.3}O_4$ samples measured at 67 K; (c) $La_{0.5}Sr_{1.5}Fe_{0.5}Ti_{0.5}O_4$ at T = 5 K, (d) distribution of hyperfine magnetic fields for $La_{0.5}Sr_{1.5}Fe_{0.5}Ti_{0.5}O_4$.

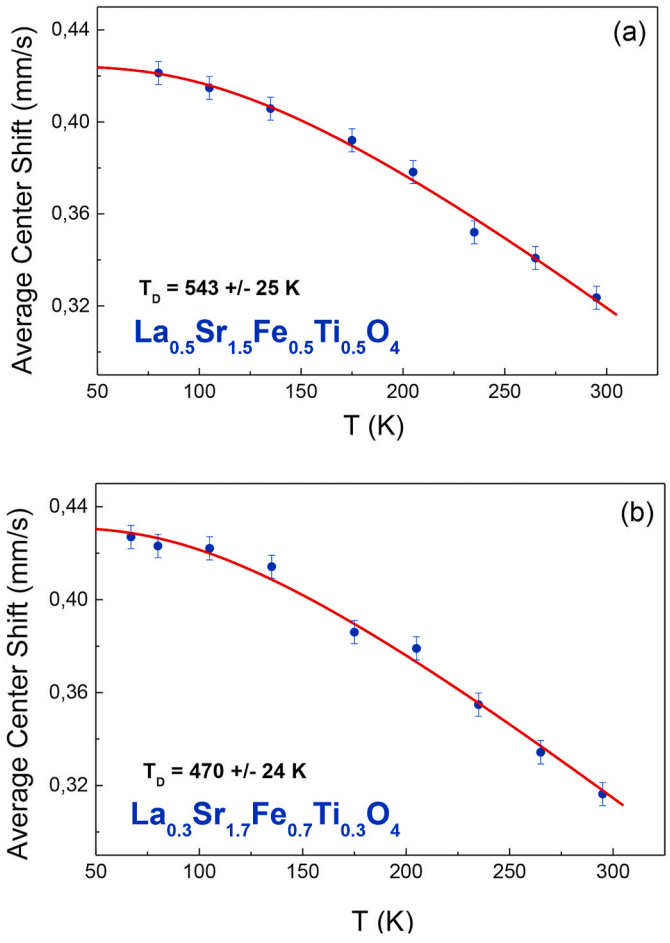

Fig. 10. Average center shift vs temperature for (a) $La_{0.5}Sr_{1.5}Fe_{0.5}Ti_{0.5}O_4$ and (b) $La_{0.7}Sr_{1.3}Fe_{0.7}Ti_{0.3}O_4$.

and it appears in FC regime, so one can suggest the presence of the uncompensated magnetic moment in one of two magnetic phases which plays the role of an external magnetic field.

Moreover, it should be noted that simultaneous existence of the high temperature antiferromagnetic correlations and the low temperature ferromagnetically correlated regions was previously observed in other perovskites, including Sr-doped systems: $YbMnO_3$, $Yb_{0.82}Sr_{0.18}MnO_3$ [24,25]. Based on electron spin resonance and magnetization measurements it was suggested that in above mentioned perovskites the ferromagnetically correlated nanoregions were formed due to the presence of mixed-valence manganese ions Mn^{3+}/Mn^{4+} and the double exchange interaction between them [24,25]. So we can suggest that in the investigated here $La_{0.5}Sr_{1.5}Fe_{0.5}Ti_{0.5}O_4$ and $La_{0.7}Sr_{1.3}Fe_{0.7}Ti_{0.3}O_4$ layered perovskites iron ions can be in different valence states, that is confirmed by Mössbauer experiments. The exchange interaction between Fe^{3+} ($3d^5$) and Fe^{4+}($3d^4$) have the complex nature and lead to the electronic phase separation.

Electron spin resonance measurements prove the possible electronic phase separation (the simultaneous existence of the paramagnetic phase and magnetically correlated regions) demonstrating two types of signals in ESR spectra (Fig. 5, Fig. S3). One can see from Fig. 6c that the integral intensity of the ESR signal from the paramagnetic phase (line 1) is two orders of magnitude higher than from magnetically correlated phase (line 2) assuming that samples are in a paramagnetic phase with a small inclusion of magnetically correlated regions that coincides with Mössbauer spectroscopy data showing only 4% of Fe^{4+} iron ions (Table 5). The change in the temperature behavior of ESR parameters was observed below 120 K in $La_{0.5}Sr_{1.5}Fe_{0.5}Ti_{0.5}O_4$ and below 150 K in $La_{0.7}Sr_{1.3}Fe_{0.7}Ti_{0.3}O_4$ that coincides with the splitting temperature of ZFC-FC curves during magnetization measurements. The shown in Fig. 6d Weiss constants were obtained from the fitting of the ESR integral intensity and they are equal to $\theta = -50$ K for $La_{0.5}Sr_{1.5}Fe_{0.5}Ti_{0.5}O_4$ and $\theta = -100$ K for $La_{0.7}Sr_{1.3}Fe_{0.7}Ti_{0.3}O_4$, respectively, confirming the presence of antiferromagnetic correlations in this phase. For $La_{0.7}Sr_{1.3}Fe_{0.7}Ti_{0.3}O_4$, this value is perfectly coincides with the Weiss constant obtained from magnetization measurements [12], while for $La_{0.5}Sr_{1.5}Fe_{0.5}Ti_{0.5}O_4$ the magnetization data can be described by the Curie - Weiss law with the Weiss constant $\theta = -50$ K (Fig. S4).

The temperature behavior of ESR parameters of line 2 in two samples coincides with the low temperature behavior of magnetization. So the typical for a ferromagnetic material increase of M_S and H_T with decreasing temperature in $La_{0.5}Sr_{1.5}Fe_{0.5}Ti_{0.5}O_4$ corresponds to the ferromagnetic nature of line 2 in ESR spectra, while for $La_{0.7}Sr_{1.3}Fe_{0.7}Ti_{0.3}O_4$ all experiments (Table 3 and Fig. 6) prove the complex nature of exchange interactions in magnetically correlated regions, which leads, for example, to ferrimagnetic ordering of the canted spin sublattices or to a helical spin structure. More detailed information on the type of magnetic ordering can be obtained in the future by the neutron powder diffraction method.

Mössbauer spectroscopy measurements were performed to investigate the valence state of iron ions in details (Figs. 7–9). The room temperature Mössbauer spectra of $La_{0.5}Sr_{1.5}Fe_{0.5}Ti_{0.5}O_4$ and $La_{0.7}Sr_{1.3}Fe_{0.7}Ti_{0.3}O_4$ samples (Fig. 7) exhibit a doublet with broadened and asymmetrical lines. The doublet structure of the Mössbauer spectra of the samples under study is retained up to low temperatures (Fig. 9). However, for the $La_{0.7}Sr_{1.3}Fe_{0.7}Ti_{0.3}O_4$ solid solution, starting from a temperature of the order of 100 K, a broadened magnetic sextet with a hypefine field of the order of 350 kOe begins to appear. At a temperature of 67 K, the hyperfine field increases to 367 kOe and the area of the sextet becomes 42%. At this temperature, a complex magnetic sextet also begins to appear in the spectrum of $La_{0.5}Sr_{1.5}Fe_{0.5}Ti_{0.5}O_4$ sample, but its area is only 10%. A further decrease of the $La_{0.5}Sr_{1.5}Fe_{0.5}Ti_{0.5}O_4$ sample temperature leads to a substantial decrease in the doublet area (up to 8%) and the appearance of a magnetic sextet with a distribution of hyperfine magnetic fields, the function of which is shown in Fig. 9d. The distribution function of hyperfine fields has a noticeable wing toward small fields and features, probably due to different numbers of ions in the environment of the Mössbauer atom.

Thus, Mössbauer measurements show that iron ions in the studied samples are in a high-spin Fe^{3+} state. The low-field wing in the distribution of hyperfine magnetic fields indicates that there are fluctuations in the exchange interaction of magnetic clusters. It should be noted that even at a temperature of about 5 K, a doublet is observed, indicating the presence of iron ions in the paramagnetic state or in superparamagnetic clusters whose blocking temperature is below 5 K. The isomer shift of this doublet (IS = 0.43 ± 0.03) corresponds to ferric ions, and is close to the average shift of the doublets at 80 K (IS = 0.421 ± 0.005). The small positive shift is probably due to the second order Doppler effect. In addition to this doublet, the spectrum of the $La_{0.5}Sr_{1.5}Fe_{0.5}Ti_{0.5}O_4$ sample at 5 K exhibits a weak broadened line with an isomer shift IS = 0.10 ± 0.1 mm/s and a relative area about 3 ± 2%. The position of this line coincides with the lines of the magnetic sextets, and therefore the parameters of this line are determined with poor statistical accuracy. Unfortunately, the superposition of this line with the lines of other doublets of Fe^{3+} ions is also observed at other temperatures of the measurements. Nevertheless, based on the results of measurements with better resolution (see Fig. 7), we believe that this line corresponds to Fe^{4+} ions. As the temperature decreases, the position of the Fe^{4+} line shifts from the region of negative velocities at room temperature to the positive velocities at low temperatures.

6. Conclusions

The single phase $La_{0.5}Sr_{1.5}Fe_{0.5}Ti_{0.5}O_4$ and $La_{0.7}Sr_{1.3}Fe_{0.7}Ti_{0.3}O_4$ layered perovskites were synthesized using a solid state method. Based on magnetization and electron spin resonance measurements one can suggest the presence of the electronic phase separation in the investigated samples – the simultaneous existence of the paramagnetic phase and magnetically correlated regions. The significant proportion of samples volume is a paramagnetic phase with strong antiferromagnetic, while the second phase is ferromagnetically correlated regions in $La_{0.5}Sr_{1.5}Fe_{0.5}Ti_{0.5}O_4$ and canted ferrimagnetically correlated regions in $La_{0.7}Sr_{1.3}Fe_{0.7}Ti_{0.3}O_4$.

The shift of the magnetic hysteresis loop was observed that is the typical manifestation of exchange bias effect due to the presence of two types of magnetic phases. The electronic phase separation can be realized due to the mixed-valence iron ions that is the presence of Fe^{4+} ions in addition to trivalent iron ions that was exactly confirmed by Mössbauer spectroscopy investigations.

CRediT authorship contribution statement

T.P. Gavrilova: Conceptualization, Methodology, Investigation, Data processing, Data curation, Writing - original draftWriting – original draft, Writing - review & editingWriting – review & editing. **A.R. Yagfarova:** Data processing. **Yu.A. Deeva:** Synthesis, Sample characterization. **I.V. Yatsyk:** Investigation, (ESR), Resources. **I.F. Gilmutdinov:** Investigation, (Magnetization), Resources. **M.A. Cherosov:** Investigation, (Magnetizaton), Resources. **F.G. Vagizov:** Investigation, (Mossbauer spectroscopy), Resources, Data curation, Writing - review & editingWriting – review & editing. **T.I. Chupakhina:** Synthesis, Sample characterization, Data curation. **R.M. Eremina:** Conceptualization, Methodology, Writing - review & editingWriting – review & editing, Supervision.

Declaration of competing interest

The authors declare that they have no known competing financial interests or personal relationships that could have appeared to influence the work reported in this paper.

Acknowledgements

Electron spin resonance measurements (T.P. Gavrilova, I.V. Yatsyk, R.M. Eremina) were performed with the financial support from the government assignment for FRC Kazan Scientific Center of RAS. Sample synthesis and the XRD analysis were supported by the state target of the Institute of Solid State Chemistry UB RAS (No AAAA-A19-119031890025-9). Magnetization measurements were supported by the subsidy allocated to Kazan Federal University for the state assignment in the sphere of scientific activities (Project No. 0671-2020-0050) Authors are grateful to the Institute of Geology and Petroleum Technologies of the Kazan (Volga region) Federal University for the study by the X-ray fluorescence analysis.

Appendix A. Supplementary data

Supplementary data to this article can be found online at https://doi.org/10.1016/j.jpcs.2021.109994.

References

[1] S. Yuvaraj, R.K. Selvan, Y.S. Lee, An overview of AB_2O_4- and A_2BO_4-structured negative electrodes for advanced Li-ion batteries, RSC Adv. 6 (2016) 21448–21474, https://doi.org/10.1039/c5ra23503k.

[2] G. Nirala, D. Yadav, Sh. Upadhyay, Ruddlesden–Popper phase A_2BO_4 oxides: recent studies on structure, electrical, dielectric, and optical properties, Journal of Advanced Ceramics 9 (2020) 129–148, https://doi.org/10.1007/s40145-020-0365-x.

[3] S. Krohns, P. Lunkenheimer, Ch. Kant, A.V. Pronin, H.B. Brom, A.A. Nugroho, M. Diantoro, A. Loidl, Colossal dielectric constant up to gigahertz at room temperature, Appl. Phys. Lett. 94 (2009) 122903 1, https://doi.org/10.1063/1.3105993. – 3.

[4] X.Q. Liu, B.W. Jia, W. Zh. Yang, J.P. Cheng, X.M. Chen, Dielectric relaxation and polaronic hopping in Al-substituted $Sm_{1.5}Sr_{0.5}NiO_4$ ceramics, J. Phys. D Appl. Phys. 43 (2010) 495402 1–6, https://doi.org/10.1088/0022-3727/43/49/495402.

[5] M.S. Wu, H.-C.I. Kao, H.S. Sheu, Y.P. Chiang, L. Horng, R.F. Hsueh, S.L. Young, W. F. Pong, J.H. Huang, Structure and properties of $(La_{2-x}Sr_x)MnO_4$ compounds, Int. J. Mod. Phys. B 19 (2005) 541–548, https://doi.org/10.1142/S0217979205029006.

[6] P.M.C. Rourke, I. Mouzopoulou, X. Xu, C. Panagopoulos, Y. Wang, B. Vignolle, C. Proust, E.V. Kurganova, U. Zeitler, Y. Tanabe, T. Adachi, Y. Koike, N.E. Hussey, Phase-fluctuating superconductivity in overdoped $La_{2-x}Sr_xCuO_4$, Nat. Phys. 7 (2011) 455–458, https://doi.org/10.1038/nphys1945.

[7] P.K. Pandey, R.J. Choudhary, D.M. Phase, Magnetic behavior of layered perovskite Sr_2CoO_4 thin film, Appl. Phys. Lett. 103 (2013) 132413, https://doi.org/10.1063/1.4823597, 1 – 5.

[8] Y. Luo, J. Zhang, Z. Yue, L. Li, Improvement in microwave dielectric properties of Sr_2TiO_4 ceramics through post-annealing treatment, J. Electroceram. 41 (2018) 67–72, https://doi.org/10.1007/s10832-018-0160-z.

[9] A. Al-Zubi, G. Bihlmayer, S. Blügel, P. Grünberg, Electronic structure of oxygen-deficient $SrTiO_3$ and Sr_2TiO_4, Crystals 9 (2019) 580, https://doi.org/10.3390/cryst9110580.

[10] Z. Lu, L. Zhang, L. Wang, Concentration dependence of luminescent properties for Sr2TiO4:Eu3+ red phosphor and its charge compensation, J. Nanomater. 2012 (2012), https://doi.org/10.1155/2012/698434.

[11] H. Zhang, S. Ni, Y. Mi, X. Xu, Ruddlesden-Popper compound Sr_2TiO_4 co-doped with La and Fe for efficient photocatalytic hydrogen production, J. Catal. 359 (2018) 112–121, https://doi.org/10.1016/j.jcat.2017.12.031.

[12] T.I. Chupakhina, N.V. Melnikova, N.I. Kadyrova, Yu.A. Deeva, A. A. Mirzorakhimov, T.P. Gavrilova, I.F. Gilmutdinov, R.M. Eremina, Synthesis, structure, magnetic behavior and dielectric relaxation of the $La_xSr_{2-x}Fe_xTi_{1-x}O_4$ (x = 0.5, 0.7) oxide ceramic, J. Solid State Chem. 292 (2020) 121687, https://doi.org/10.1016/j.jssc.2020.121687, 1 – 12.

[13] Yu.A. Deeva, T.I. Chupakhina, N.V. Melnikova, A.A. Mirzorakhimov, Dielectric properties of new oxide phases $Ln_{0.65}Sr_{1.35}Co_{0.5}Ti_{0.5}O_4$ (Ln = La, Nd, Pr) with the K_2NiF_4 - type structure, Ceram. Int. 46 (2020) 15305–15313, https://doi.org/10.1016/j.ceramint.2020.03.071.

[14] M.E. Matsnev, V.S. Rusakov, SpectrRelax: an application for Mossbauer spectra modeling and fitting, Am. Inst. Phys. Conf. Proc. 1489 (2012) 178–185, https://doi.org/10.1063/1.4759488.

[15] A.L. Geiler, V.G. Harris, C. Vittoria, N.X. Sun, A quantitative model for the nonlinear response of fluxgate magnetometers, J. Appl. Phys. 99 (2006), https://doi.org/10.1063/1.2170061.

[16] R.M. Eremina, I.V. Yatsyk, A.V. Shestakov, I.I. Fazlizhanov, T.P. Gavrilova, F. O. Milovich, A.L. Zinnatullin, F.G. Vagizov, I.F. Gilmutdinov, P.S. Shirshnev, D. I. Sobolev, N.V. Nikonorov, Observation of ε - Fe_2O_3 nanoparticles precipitated in potassium aluminoborate glasses doped with 4 mol % Fe_2O_3, J. Phys. Chem. Solid. 133 (2019) 7–14, https://doi.org/10.1016/j.jpcs.2019.04.027.

[17] A. Abragam, B. Bleaney, Electron Paramagnetic Resonance of Transition Ions, Oxford University Press, 1970.

[18] J. Deisenhofer, R.M. Eremina, A. Pimenov, T. Gavrilova, H. Berger, M. Johnsson, P. Lemmens, H.-A. Krug von Nidda, A. Loidl, K.-S. Lee, M.-H. Whangbo, Structural and magnetic dimers in the spin-gapped system $CuTe_2O_5$, Phys. Rev. B 74 (2006) 174421 1–8, https://doi.org/10.1103/PhysRevB.74.174421.

[19] Z. Seidov, T.P. Gavrilova, R.M. Eremina, L.E. Svistov, A.A. Bush, A. Loidl, H.-A. Krug von Nidda, Anisotropic exchange in $LiCu_2O_2$, Phys. Rev. B 95 (2017), https://doi.org/10.1103/PhysRevB.95.224411.

[20] S.E. Dann, M.T. Weller, D.B. Currie, M.F. Thomas, A.D. Al-Rawwas, Structure and magnetic properties of Sr2FeO4 and Sr3Fe2O7 studied by powder neutron diffraction and Mössbauer spectroscopy, J. Mater. Chem. 3 (1993) 1231–1237, https://doi.org/10.1039/JM9930301231.

[21] Yi-Long Chen, De-Ping Yang, Mössbauer Effect in Lattice Dynamics: Experimental Techniques and Applications, WILEY-VCH Verlag GmbH & Co. KGaA, 2007.

[22] G.K. Wertheim, Mossbauer Effect: Principles and Applications, Academic Press, New York, 1964.

[23] P.K. Manna, S.M. Yusuf, Two interface effects: exchange bias and magnetic proximity, Phys. Rep. 535 (2014) 61–99, https://doi.org/10.1016/j.physrep.2013.10.002.

[24] R.M. Eremina, T.P. Gavrilova, I.V. Yatsyk, R.B. Zaripov, A.A. Sukhanov, V. A. Shustov, N.M. Lyadov, V.I. Chichkov, N.V. Andreev, Magnetic resonance investigations of h-$YbMnO_3$, Appl. Magn. Reson. 47 (2016) 869–879, https://doi.org/10.1007/s00723-016-0798-0.

[25] E.O. Bykov, T.P. Gavrilova, I.V. Yatsyk, I.F. Gilmutdinov, V.V. Parfenov, A. I. Kurbakov, R.M. Eremina, Structural and magnetic properties of $Yb_{1-x}Sr_xMnO_3$, Ceram. Int. 45 (2019) 10286–10294, https://doi.org/10.1016/j.ceramint.2019.02.083.